Earth and Planetary Science Letters 585 (2022) 117527

Contents lists available at ScienceDirect

Earth and Planetary Science Letters

www.elsevier.com/locate/epsl

Co-variation systematics of uranium and molybdenum isotopes reveal pathways for descent into euxinia in Mediterranean sapropels

Chun Fung Chiu [a,*], Tim C. Sweere [a], Matthew O. Clarkson [a], Gregory F. de Souza [a], Rick Hennekam [a,b], Derek Vance [a]

[a] ETH Zurich, Institute of Geochemistry and Petrology, Clausiusstrasse 25, 8092 Zurich, Switzerland
[b] NIOZ Royal Netherlands Institute for Sea Research, Department of Ocean Sciences, 't Horntje 1797 SZ, the Netherlands

ARTICLE INFO

Article history:
Received 14 December 2021
Received in revised form 25 March 2022
Accepted 1 April 2022
Available online 11 April 2022
Editor: F. Moynier

Keywords:
redox
molybdenum isotopes
uranium isotopes
sapropels
Eastern Mediterranean

ABSTRACT

The elemental concentrations and isotope compositions of molybdenum (Mo) and uranium (U) are commonly used for the reconstruction of past global and local redox conditions, and recent studies using both elements have revealed the potential of their paired application. However, such studies have generally focused either on modern marine sediments or on relatively low-resolution reconstructions of deep-time paleo-redox conditions. Here, we present high-resolution profiles (every 0.2-0.3 kyr) of Mo and U elemental and isotope compositions for anoxic organic-rich sediments of Eastern Mediterranean sapropels S5 and S7. The new Mo-U data reveal the processes leading to descent into basinal euxinia in more precise and systematic detail than lower resolution datasets focused on either Mo or U only.

During the intensification from anoxic non-sulfidic to persistently euxinic conditions, δ^{98}Mo and δ^{238}U covariation systematics exhibit two stages. We identify the Mo-U isotope signature of the early transition from anoxic non-sulfidic to mildly euxinic conditions in the first stage, characterized by a rise in U isotope ratios (from -0.3‰ to $+0.2$‰ ± 0.05‰) controlled by the depth within the sediment of the uranium reduction-accumulation front. As the water column turns persistently euxinic, δ^{98}Mo values approach the seawater value for both sapropels, but δ^{238}U evolves to different final values in the two sapropels. We interpret these differences as reflecting different redox potentials and/or different degrees of restriction of these two sapropel events, and the more gradual response of U sequestration to redox variation in comparison with threshold behavior of Mo. The findings presented here show temporal patterns in δ^{98}Mo and δ^{238}U on relatively short timescales that suggest the combined use of these proxies at high resolution allows detailed reconstruction of local redox and hydrographic conditions.

1. Introduction

Reconstructing oceanic redox history has long been the interest of geoscientists because of its close association with the evolution of life and Earth's atmosphere. Molybdenum (Mo) and uranium (U) concentrations and isotope compositions are powerful tools for such reconstructions. Both elements are well studied in the modern ocean and its sediments (see reviews by Andersen et al., 2017; Kendall et al., 2017, and references therein). In the modern well-oxygenated ocean, both Mo and U behave conservatively, with long ocean residence times of ~400-500 kyr (Dunk et al., 2002; Miller et al., 2011). They are dominantly present in the soluble forms - molybdate ions and uranyl complexes respectively (Emerson and Huested, 1991; Dunk et al., 2002). However, under reducing conditions both are much more easily removed from the dissolved pool. Recent studies of modern marine sediments have particularly highlighted the potential of combined Mo and U abundance and isotope analysis, given their differential sensitivities to a number of output processes, to provide a more detailed understanding of redox and its evolution (e.g. Noordmann et al., 2015; Bura-Nakić et al., 2018; Brüske et al., 2020).

Under oxic conditions, adsorption onto manganese and iron oxyhydroxide minerals is the dominant removal pathway of Mo, a process that preferentially incorporates light Mo isotopes into the particulate phase, with a fractionation factor of up to -3‰ relative to seawater (Barling and Anbar, 2004; Goldberg et al., 2009; Wasylenki et al., 2008). By contrast, in euxinic conditions, molybdate (MoO_4^{2-}) reacts with dissolved H_2S to form thiomolybdates, which are particle-reactive and rapidly removed to sediments, either via scavenging by pyrite and organic matter, or formation of

* Corresponding author.
E-mail address: fuchiu@ethz.ch (C.F. Chiu).

https://doi.org/10.1016/j.epsl.2022.117527

particulate Fe-Mo-S phases (Chappaz et al., 2014; Helz and Vorlicek, 2019). Under strongly euxinic conditions, the conversion of MoO_4^{2-} to MoS_4^{2-} (tetrathiomolybdate) is nearly complete, such that little isotope fractionation is expressed. Sediments deposited under strongly euxinic conditions therefore approach the seawater δ^{98}Mo value (e.g. Nägler et al., 2011; Bura-Nakić et al., 2018; Brüske et al., 2020). Under weakly euxinic conditions, the conversion of molybdate to thiomolybdates is incomplete, and more sulfidized thiomolybdate species are progressively isotopically lighter (Tossel, 2005; Kerl et al., 2017). δ^{98}Mo values of sediments deposited under such conditions usually vary between $-0.6‰$ and $+1.8‰$, lighter than the modern seawater value of $+2.34‰$ (e.g. Neubert et al., 2008; Poulson-Brucker et al., 2009; Nägler et al., 2011), and can be modeled by the kinetically controlled preferential scavenging of the more sulfidized thiomolybdate species (Dahl et al., 2010; Matthews et al., 2017; Sweere et al., 2021).

Under anoxic conditions, with redox potential below the Fe(III)-Fe(II) transition (Zheng et al., 2002), highly soluble U(VI) can be reduced to U(IV) and buried in the form of insoluble minerals (Anderson et al., 1989; Algeo and Tribovillard, 2009). Although the precise reduction pathway is poorly understood, U reduction can be mediated by metal- and sulfate-reducing bacteria on particle surfaces, or occur abiotically (e.g. Stylo et al., 2015). These circumstances cause U reduction mostly in sediment, rather than in the water column (Anderson et al., 1989). Most authigenic U in marine sediment is thus supplied via diffusion of water-column U into pore water, driven by a concentration gradient resulting from sedimentary U reduction. Additionally, U scavenging by sinking particulate organic matter is a minor vector for authigenic U (Anderson et al., 1989; Bura-Nakić et al., 2018). Typically, ^{238}U is preferentially removed into U(IV), with an intrinsic fractionation factor of $\sim +1.2‰$ (Andersen et al., 2014). However, since U reduction takes place within the sediment, the diffusive supply of dissolved U suppresses the fractionation expressed (Andersen et al., 2014). Hence, the isotopic offset from seawater is typically limited to half of the intrinsic fractionation factor, i.e. $+0.6‰$, when U removal starts at the sediment-water interface (Andersen et al., 2014). Andersen et al. (2014) also describe additional potential sedimentary U isotope signatures related to U reduction fronts at levels beneath the sediment-water interface, and to basinal restriction.

In summary, while Mo and U and their isotope compositions in authigenic sedimentary phases are both sensitive to changes in redox state, the differences in their geochemical sensitivities and isotope fractionation behavior mean that each records unique chemical and temporal aspects of redox evolution. Whilst a number of studies of modern and ancient sediments (e.g. Kendall et al., 2015; Noordmann et al., 2015; Bura-Nakić et al., 2018; Brüske et al., 2020) have highlighted the utility of these combined isotope systems, they have often captured a low-resolution snapshot of local redox dynamics. Here, we examine the covariation of the Mo and U isotope systems over a well-defined temporal progression of redox states. To this end, we present high-resolution (1 sample per ~200-300 years) records of Mo and U concentration and isotope data for two chronologically well-constrained intervals of Pleistocene deoxygenation in the Eastern Mediterranean Sea sapropel events, S5 and S7, data that complements existing δ^{98}Mo data (Sweere et al., 2021). We interpret the temporal evolution of δ^{238}U and δ^{98}Mo in the context of other trace metal data, and place special focus on the co-variation of these two isotope proxies, discussing the complementary information on early versus late paleo-redox evolution that the two systems provide as a consequence of their differing geochemistry. Finally, we identify general systematics of isotope co-variation in the context of basinal deep-water renewal and redox evolution, providing a framework for interpreting similar datasets in older sediments.

2. Study site & methods

2.1. Mediterranean sapropels

Eastern Mediterranean sapropels are organic-rich sediments deposited during intervals of anoxic bottom water conditions, resulting from increased export productivity and/or enhanced organic matter preservation (e.g. de Lange et al., 2008; Rohling et al., 2015). Their occurrence coincided with insolation maxima in the Northern Hemisphere related to the precession cycle, with the associated stronger monsoon driving greater freshwater supply from North Africa to the Eastern Mediterranean (e.g. see review in Rohling et al., 2015). Such a flux of less dense and nutrient-rich freshwater would both stimulate productivity and strengthen water-column stratification, processes that increase deep oxygen demand and reduce oxygen supply, thus encouraging development of anoxia.

Sapropels S5 (~128.3-121.5 kyr BP; Grant et al., 2016) and S7 (~198.5-191.9 kyr BP; Ziegler et al., 2010) are strongly developed Mediterranean sapropels. Previous studies, based on the inverse correlation between Fe/Al and δ^{56}Fe and seawater-like δ^{98}Mo values, have identified euxinic (i.e. presence of H_2S) water columns during the peak stages of these two sapropel events (Andersen et al., 2018; Benkovitz et al., 2020; Sweere et al., 2021). Good preservation of these two Mediterranean sapropels, as well as their recent formation, allow exceptional age constraints (Grant et al., 2016; Ziegler et al., 2010) and favor the faithful recording of isotopic signatures after sedimentation and early diagenesis. Additionally, the basin conditions during these two sapropel events have been reasonably well-constrained by previous studies using a range of proxies (e.g. Melki et al., 2010; Benkovitz et al., 2020). At their peaks, sapropels S5 and S7 are the strongest sapropels of at least the last 250 kyr, but their development and demise see a wide range of local redox conditions, from oxic to strongly euxinic, within relatively short timescales (e.g. Benkovitz et al., 2020; Sweere et al., 2021). They thus provide excellent case studies to examine Mo-U fractionation behavior and their interrelationship, and in particular the potential utility of the combined use of Mo- and U-isotope systematics to document the temporal development of anoxic conditions (e.g. Andersen et al., 2020). Indeed, recent sapropel studies using δ^{98}Mo and δ^{238}U, together with Mo-U enrichments, have successfully identified strengthening water-column euxinia throughout S5 (Andersen et al., 2018), and weakly euxinic conditions with rapid development of anoxia at the beginning of S1 (~10.5–6.1 kyr BP, Grant et al., 2016) at a deeper coring site (ODP967, Andersen et al., 2020).

2.2. Core settings and age models

All samples in this study come from a 920.5 cm long piston core, 64PE406-E1, retrieved in January 2016 by R/V *Pelagia* during research cruise 64PE406 of the Netherlands Earth System Science Centre. The core was taken from a water depth of 1760 m in the southeastern Levantine Sea (33°18.15′N, 33°23.72′E; Fig. 1). The core chronology for the last 250 kyr is constructed using the well-dated sapropel boundaries (Grant et al., 2016; Ziegler et al., 2010), detectable using Ba and Ba/Al excursions (see Hennekam et al., 2020 for details). Ages are linearly interpolated from sapropel boundaries.

2.3. Sample processing and analytical methods

The study presents U concentration and stable isotope composition data for 30 samples, from S5 and S7, for which elemental and Mo isotope compositions were recently reported by Sweere et al. (2021). We also report Mo and U concentration and isotopic data

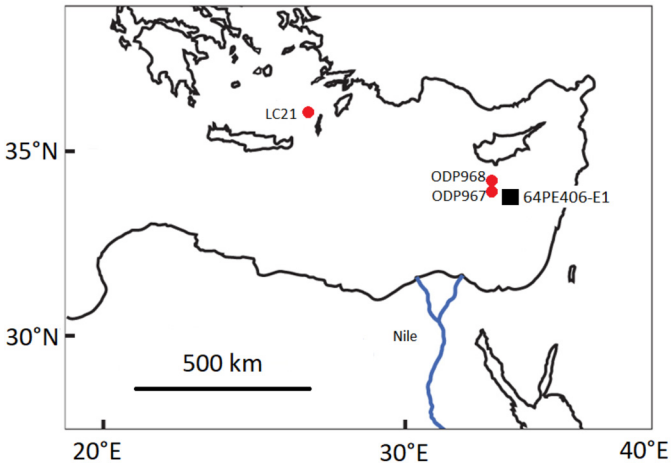

Fig. 1. Locations of the core 64PE406-E1 (this study), core ODP967 studied by Andersen et al. (2018) and Benkovitz et al. (2020), and cores ODP968 and LC21 used in the age model.

for 29 more samples in order to attain 1-cm sample resolution across both sapropel events. These new samples were first dried and powdered. About 50 mg of powdered sample was then dissolved, first using a concentrated HNO_3-HF (3:1) mixture, followed by concentrated HNO_3-HCl (3:2) mixture. The dissolved sample was dried down and re-dissolved in 2.5 mL concentrated HNO_3, before being diluted by factor 1250 in 2% HNO_3 for concentration analysis by Thermo-Finnigan *Element XR* ICP-MS. An internal In standard was used to correct for instrumental drift. Repeated analysis of secondary standard SLRS-6 (n=8) was used to constrain analytical precision, giving 2 standard deviations (SD) of 5% for all elemental data presented here, except Fe, which has 2SD precision of 6%.

For the isotopic analysis, aliquots containing 50 – 300 ng U were spiked with IRMM-3636 U double-spike (Richter et al., 2008). Samples for which Mo isotopes were also analyzed were additionally spiked with ^{100}Mo–^{97}Mo double-spike (Archer and Vance, 2008). The dried sample-spike mixture was redissolved in 1 mL 1 M HCl and these solutions were then refluxed for at least one hour to equilibrate, before column chromatography. Chromatographic separation is modified from Bura-Nakić et al. (2018), with two column passes and using a smaller load volume. The collected solution containing Mo or U was dried down and refluxed in a concentrated HNO_3-H_2O_2 mixture, before being dried down again. The purified Mo and U fractions were redissolved in 2% HNO_3 and 0.2M HCl respectively for isotopic analysis.

Mo and U isotopes were measured on a Thermo-Fisher *Neptune Plus* MC-ICP-MS using a PFA nebulizer and spray chamber fitted to an Aridus II auto-sampler (CETAC). Measurements were made at low mass resolving power ($M/\Delta M \approx 500$), and 'standard cones' were used for Mo. For uranium, most measurements were made using an 'X-cone' and standard sample cone, but some samples were measured using the 'X+Jet' cone setup.

Mo isotope compositions are expressed as $\delta^{98}Mo$, relative to a value of +0.25‰ for the standard NIST SRM-3134:

$$\delta^{98}\mathrm{Mo(in‰)} = \left[\frac{(^{98}\mathrm{Mo}/^{95}\mathrm{Mo})_{\mathrm{sample}}}{(^{98}\mathrm{Mo}/^{95}\mathrm{Mo})_{\mathrm{NIST\ SRM-3134}}} - 1\right] \times 1000 + 0.25 \quad (1)$$

Uranium isotope ratios $^{238}U/^{235}U$ are reported relative to standard CRM-145:

$$\delta^{238}\mathrm{U(in‰)} = \left[\frac{(^{238}\mathrm{U}/^{235}\mathrm{U})_{\mathrm{sample}}}{(^{238}\mathrm{U}/^{235}\mathrm{U})_{\mathrm{CRM-145}}} - 1\right] \times 1000 \quad (2)$$

Internal uncertainties were 0.02–0.07‰ for $\delta^{98}Mo$. The external reproducibility was constrained via replicate measurements of NIST SRM-3134 (±0.04‰, 2SD, n=17). Internal uncertainties were 0.02-0.04‰ for $\delta^{238}U$. External uncertainty was obtained via multiple analyses of the uraninite standard CZ-1 (purified in the same manner as samples, run every 5 samples in the same session as the samples and at a similar concentrations), yielding ±0.04 to ±0.07, depending on the cone setup used. Replicate measurements of the SDO-1 shale standard, using both cone setups, gave an average of −0.08 ± 0.05‰ (2SD, n=8) during the measurement period, within error of published values (Kendall et al., 2015). Unless the internal error is greater, the external reproducibility is assigned as the error reported in Table S1 and all figures.

Sedimentary total organic carbon (TOC) contents were determined using a ThermoFisher Flash-EA 1112 coupled to a ThermoFisher Delta V isotope ratio mass spectrometer via a Conflo IV interface, after dissolution of carbonates in 6M HCl for at least 24 hours.

2.4. Estimation of authigenic fractions

To correct for contributions from detrital minerals, the enrichment factors and authigenic concentrations of Mo and U are calculated as follows:

$$X_{EF} = \frac{(X/Al)_{sample}}{(X/Al)_{detr}}, \quad (3)$$

where X and Al represent the mass concentrations of element X and Al, and

$$\mathrm{Mo_{detr}} = [\mathrm{Mo}]_{\mathrm{bulk}} - \left(\frac{\mathrm{Mo}}{\mathrm{Al}}\right)_{\mathrm{detr}} \times [\mathrm{Al}]_{\mathrm{sample}} \quad (4)$$

$$\mathrm{U_{detr}} = [\mathrm{U}]_{\mathrm{bulk}} - \left(\frac{\mathrm{U}}{\mathrm{Al}}\right)_{\mathrm{detr}} \times [\mathrm{Al}]_{\mathrm{sample}} \quad (5)$$

For these calculations, we use the detrital ratios $= 20 \times 10^{-6}$ g/g for Mo/Al and 26.5×10^{-6} g/g for U/Al based on the ratios found in background sediments outside the sapropel events (Clarkson et al., 2021, TS unpublished data).

The isotope compositions of the authigenic material are calculated from mass balance as follows:

$$\delta^{98}\mathrm{Mo_{auth}} = \frac{\delta^{98}\mathrm{Mo_{bulk}} \times [\mathrm{Mo}]_{\mathrm{bulk}} - \delta^{98}\mathrm{Mo_{detr}} \times [\mathrm{Mo}]_{\mathrm{detr}}}{[\mathrm{Mo}]_{\mathrm{auth}}} \quad (6)$$

and

$$\delta^{238}\mathrm{U_{auth}} = \frac{\delta^{238}\mathrm{U_{bulk}} \times [\mathrm{U}]_{\mathrm{bulk}} - \delta^{238}\mathrm{U_{detr}} \times [\mathrm{U}]_{\mathrm{detr}}}{[\mathrm{U}]_{\mathrm{auth}}} \quad (7)$$

where the average continental crust isotope ratios are used as reference values for the detrital composition, i.e. + 0.3‰ for $\delta^{98}Mo_{detr}$ and – 0.3‰ for $\delta^{238}U_{detr}$ (see reviews in Kendall et al., 2017 and Andersen et al., 2017 respectively). Authigenic isotope compositions for three samples with bulk Mo/Al within a factor of 3 of the detrital value have very large uncertainties and are not shown on figures (see Supplementary Data Table).

3. Results

The full concentration and isotope dataset are presented in the Supplementary Table. Fig. 2 shows trace element and TOC data for sapropel events S5 and S7 in core 64PE406-E1. The sapropel boundaries are defined based on the Ba/Al data, with the sapropel onset given by the first increase of Ba/Al above detrital background values, coinciding with a rise in TOC. The end of the sapropel intervals is defined by a large drop in Ba/Al towards detrital background

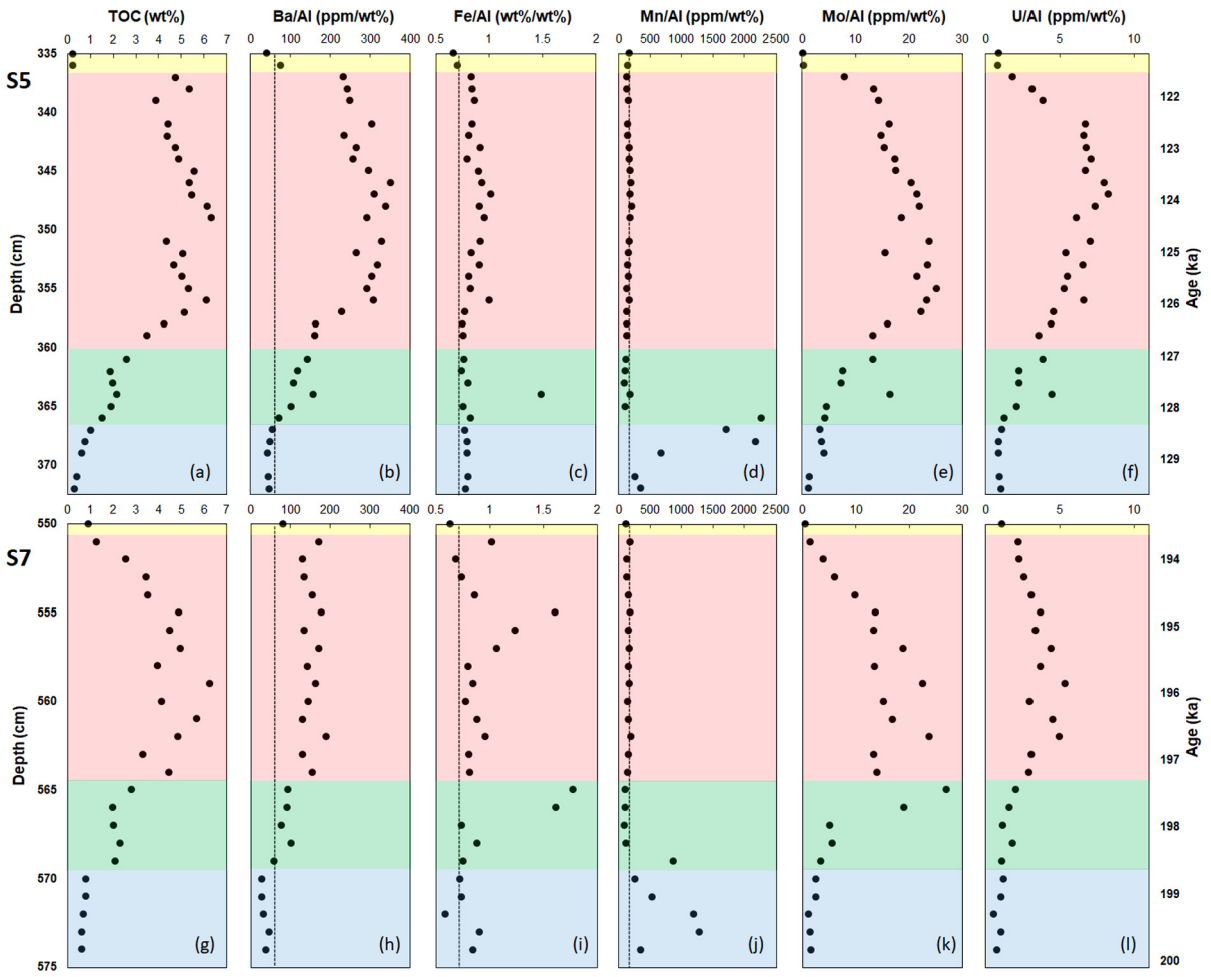

Fig. 2. TOC and elemental profiles across sapropels S5 and S7 in core 64PE406-E1. Background colors follow Ba/Al-based sapropel boundaries and a TOC-based subdivision of the sapropel (Section 3). Dashed lines in Ba/Al and Fe/Al profiles mark the corresponding average ratios from an Eastern Mediterranean core ODP967 in the vicinity of 64PE406-E1 (Wehausen and Brumsack, 1999; Benkovitz et al., 2020), while dashed lines in Mn/Al profiles refer to average Mn/Al from PAAS (Tribovillard et al., 2006). (For interpretation of the colors in the figure(s), the reader is referred to the web version of this article.)

values and coincide with TOC dropping below 1%. To further aid discussion of the data, the sapropel intervals were subdivided into *early sapropel* (<3% TOC) and *late sapropel* (>3% TOC) — based on a marked rise in TOC contents during both sapropels (Fig. 2).

Fe/Al values (Fig. 2c,i) in almost all sapropel samples are elevated relative to the average background value of 0.724 g/g from nearby core ODP967 (Benkovitz et al., 2020). In general, late sapropels have slightly higher Fe/Al than pre- and post-sapropels. A few anomalously high Fe/Al values are observed in both early sapropels and in late S7. Mn/Al values (Fig. 2d, j) are elevated above background values in the pre-sapropel stage and the lower part of the early sapropel stage, with these elevations occurring stratigraphically below the Fe/Al peaks.

Concentrations of authigenic Mo are below 25 ppm in pre-sapropels, followed by a rise to maxima over 150 ppm in the late stage of both S5 and S7 (Fig. 3a, e). $[Mo]_{auth}$ then decreases to below 100 ppm in the upper late stage, and further to below 5 ppm in the post-sapropel stage. Peaks in $[Mo]_{auth}$ coincide with Fe/Al anomalies in the early phase of both sapropels (Fig. 2). Patterns of variation in $\delta^{98}Mo_{auth}$ are similar for S5 and S7 (Fig. 3c,g), with moderate values between +0.6 and +1.6‰ in pre-sapropels before a decrease at the sapropel onset. Excursions (up to > +2‰ in S5 and down to −1.5‰ in S7; Fig. 3c and g respectively) coincide with peaks in both Fe/Al and $[Mo]_{auth}$ (Figs. 2c,i; 3a,e). Above these excursions, $\delta^{98}Mo_{auth}$ values progressively rise to above +2.0‰ in the early late sapropel stage and stay steady at this value throughout most of the late and post-sapropel stages.

$[U]_{auth}$ in S5 rises from ~3 ppm in the pre-sapropel stage (Fig. 3b, f), reaching a plateau of ~40 ppm in the late stage. For S7, $[U]_{auth}$ is generally lower, between 15 and 40 ppm. Values of $\delta^{238}U_{auth}$ gradually increase from values below −0.2‰ in the pre- and early sapropel stages of both events (Fig. 3d,h). In the late S5, $\delta^{238}U_{auth}$ decreases from a maximum of 0±0.1 ‰ near the bottom, before returning to ~0‰, followed by a drop back to −0.16‰ in post-S5. By contrast, $\delta^{238}U_{auth}$ in S7 remains between +0.1‰ and +0.35‰ throughout the late and post-sapropel stages.

4. Discussion

4.1. Redox conditions indicated by elemental enrichments

Trace element and TOC concentration data can provide a first indication of the development of reducing conditions during sapropel events. In general, TOC contents, concentrations and Al-normalized ratios of Ba, Mo, and U increase from low values in the pre-sapropel stages and reach a peak in the late stages (Fig. 2), the latter marking the most intense reducing conditions (e.g. Tribovillard et al., 2006). By contrast, elevated Mn/Al ratios are found close to the onset of sapropel events (Fig. 2d, j). Similar Mn enrichments have been found after periodic oxygenation in the Baltic Deeps, due to precipitation of Mn carbonate from Mn sourced from the

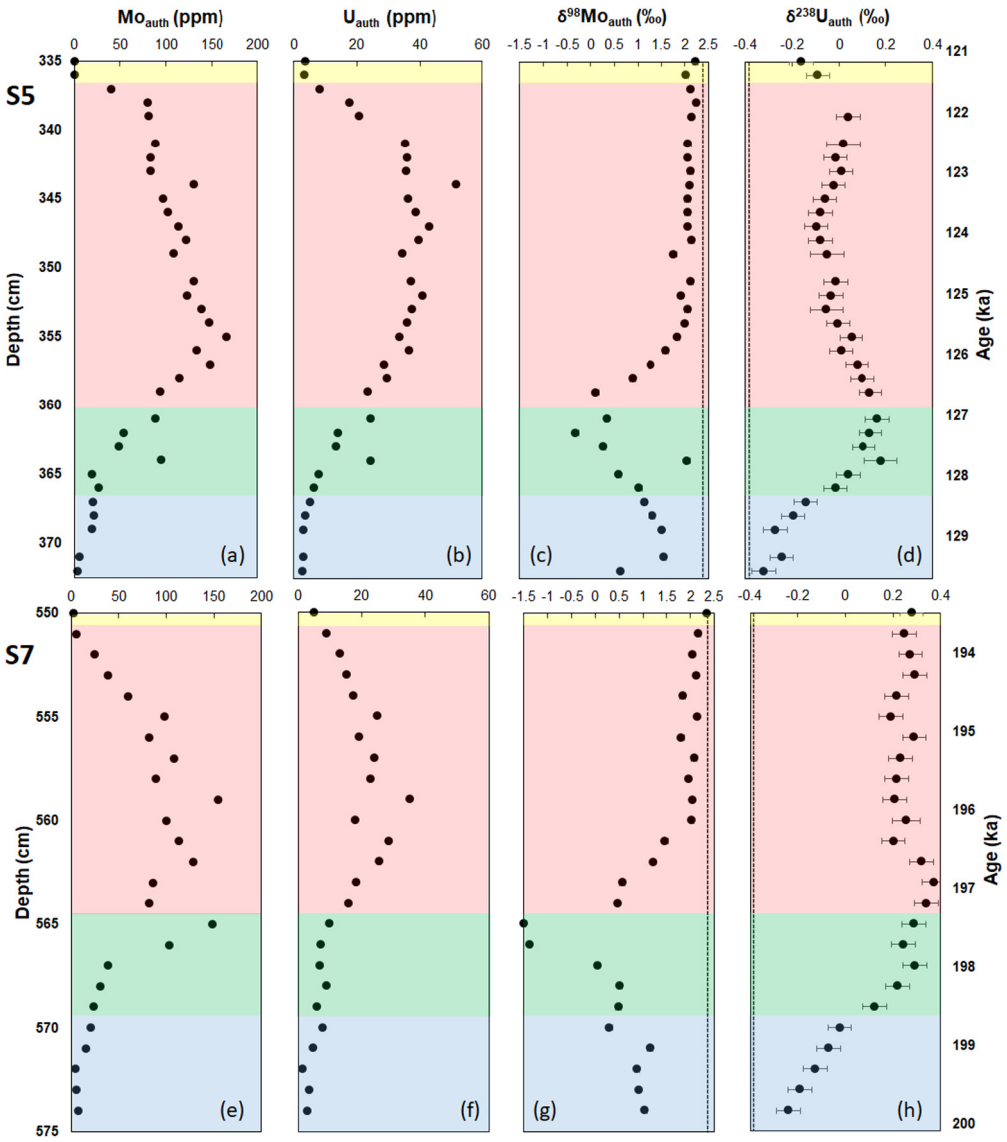

Fig. 3. Depth and age profiles for concentrations and isotope compositions of authigenic Mo and U. Background colors follow Ba/Al-based sapropel boundaries and a TOC-based subdivision of the sapropel (Section 3). The open-ocean isotope compositions of Mo and U are represented as dashed lines.

reductive dissolution of Mn oxyhydroxides as conditions return to anoxia (Huckriede and Meischner, 1996). The high Mn/Al ratios observed in the lower sections of S5 and S7 may result from a similar process, in which case the Mn-enriched sections would represent a transition from oxic to anoxic conditions during the early phase of these sapropel events. Alternatively, these high Mn/Al values may reflect remobilization of Mn from the anoxic sapropel and reprecipitation in the underlying organic carbon-free sediment (e.g. van Santvoort et al., 1996).

Above the Mn-rich sediments, Fe/Al and $[Mo]_{auth}$ peaks are observed (Fig. 2, 3), consistent with active Fe shuttling in the basin as suggested by published Fe isotope data for S5 and S7 from a deeper site ODP967 (2550 mbsl) (Benkovitz et al., 2020). At the onset of euxinia, water-column euxinia was likely spatially limited such that the ratio of oxic (Fe source) to euxinic area (sink) was high (Lyons and Severmann, 2006). Focusing of shuttled Fe into sediments below euxinic waters could give rise to the observed Fe/Al peaks, which in this case may roughly indicate the onset of euxinic conditions in the deep water. The focusing may also explain the very high $[Mo]_{auth}$, enhancing Mo removal via pyrite uptake (Chappaz et al., 2014) and/or formation of Fe-Mo-S particulates (Helz et al., 2011; Helz and Vorlicek, 2019). Elevated Fe/Al ratios for the rest of the samples, above background Mediterranean values (Fig. 2c,i), suggest persistent anoxia and the enhanced formation of iron-bearing minerals (Lyons and Severmann, 2006).

Concentrations of authigenic Mo and U (Fig. 3) and their Al-normalized ratios (Fig. 2e,f,k,l) follow the general increase observed for TOC contents, Ba/Al, and Fe/Al. The co-evolution of authigenic Mo and U across the two events can be summarized using an enrichment factor (EF) plot (Algeo and Tribovillard, 2009), shown in Fig. 4. Pre- and post-sapropel sediments, together with most of the early sapropel samples, have moderate EFs, suggesting non-sulfidic conditions (Algeo and Tribovillard, 2009). Above the Mn-enriched early stages of S5 and S7, the Mo_{EF}-U_{EF} data display trends parallel to seawater Mo/U (Fig. 4), lying between the characteristic patterns of Mo_{EF}–U_{EF} covariation under open marine settings and strongly restricted settings such as the Black Sea (Algeo and Tribovillard, 2009). This trend is broadly similar to the S5 and S7 trajectories discussed in Benkovitz et al. (2020). The intermediate trajectory, implying higher Mo supply relative to U than e.g. for the Black Sea, could be explained by greater supply of Mo relative to U via supply of particulate oxides from the oxic margin, with their dissolution in the euxinic basin feeding the sulfidised Mo pool. Finally, Mo/U ratios in S5 decrease slightly with increasing Mo-U enrichment, as

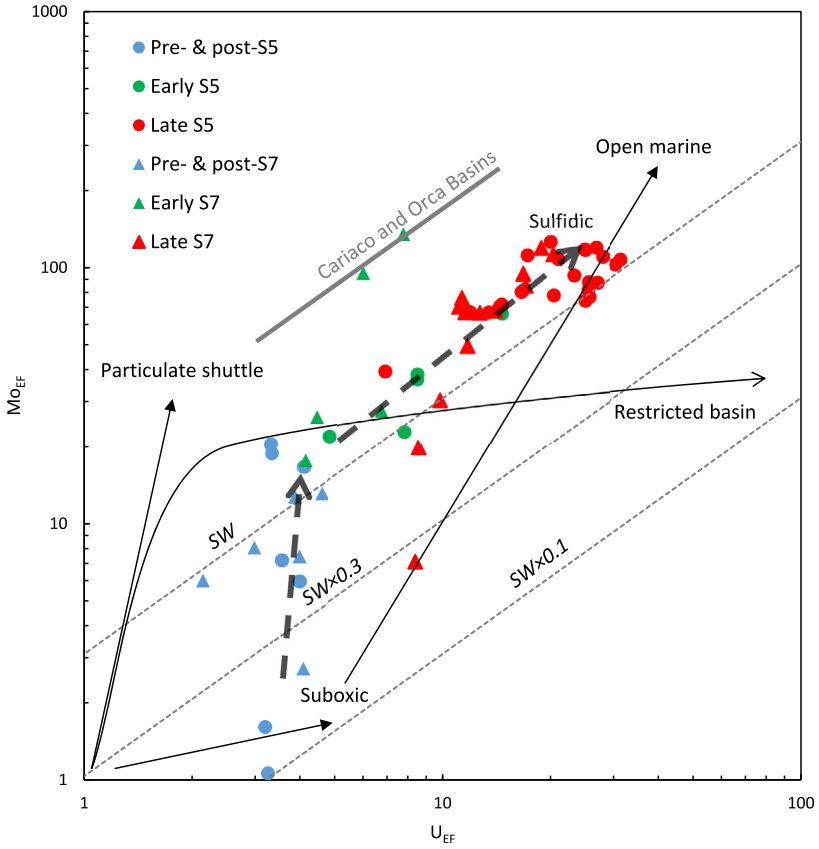

Fig. 4. Plot of enrichment factors (EF) of Mo and U from sapropels S5 and S7. Circles and triangles represent S5 and S7 data respectively. The dashed lines mark the trends along seawater Mo_{EF}/U_{EF} ratio (SW), 0.3 × seawater ratio ($0.3 \times SW$), and 0.1 × seawater ratio ($0.1 \times SW$). The black arrows show schematic evolution in enrichment factors trajectories based on three characteristic settings (open marine, particulate shuttle, and restricted basin), as presented by Algeo and Tribovillard (2009). The dotted arrows roughly indicate the evolution of our data. The gray solid line represents the main covariant trend of Mo_{EF} versus U_{EF} from Cariaco and Orca basins where "particulate shuttle" is in operation (Algeo and Tribovillard, 2009).

revealed by a slight downward deflection of the S5 trajectory in its late stages, a feature that is absent in S7 (Fig. 4). This difference may be ascribed to a lower deep-water renewal rate in S5 than in S7, leading to a more pronounced drawdown of the water-column Mo inventory during S5. Hence, Fe/Al and Mo_{EF}–U_{EF} data identify that both sapropel events began with anoxic non-sulfidic conditions during pre-sapropel stages followed by transition to euxinic conditions in the late sapropel stages. Low $[Mo]_{auth}$ and $[U]_{auth}$ in the final post-sapropel stages suggest that bottom-water conditions then returned to non-euxinic.

4.2. Behavior of molybdenum and δ^{98}Mo during sapropel events

There are clear similarities in the stratigraphic evolution of $\delta^{98}Mo_{auth}$ and $[Mo]_{auth}$ through both sapropel events at site 64PE406-E1, and S5 shows comparable trends to published data from site ODP967C (Andersen et al., 2018). This overall trend is illustrated in Fig. 5. As discussed by Sweere et al. (2021), the data reflect a general trend toward increasingly sulfidic conditions in the basin during the progression to late sapropel stages. Pre-sapropel intervals show low (<25 ppm) Mo concentrations coupled to intermediate $\delta^{98}Mo_{auth}$ values (+0.3 to +1.6‰), suggesting deposition in non-euxinic conditions (Scott and Lyons, 2012; Matthews et al., 2017; Sweere et al., 2021). Considering the high Mn concentrations for this interval, isotopically light Mo originally deposited in association with Mn oxides could contribute to the intermediate $\delta^{98}Mo_{auth}$ values (e.g. Reitz et al., 2007). Reductive dissolution of Mn oxides may have released isotopically light Mo (as low as −0.7‰, Barling and Anbar, 2004) to pore waters that, mixed with isotopically heavier Mo derived from seawater, could create the observed intermediate $\delta^{98}Mo_{auth}$ values.

Subsequently, rising $[Mo]_{auth}$ and a drop in $\delta^{98}Mo_{auth}$ values during early sapropel intervals likely reflect the onset of euxinic conditions, with a large isotopic fractionation between sediments and seawater — resulting from incomplete molybdate-to-thiomolybdate conversion — preserved in mildly euxinic conditions (Matthews et al., 2017; Sweere et al., 2021). For the early sapropel interval of S7, the new higher-resolution data reveal a brief excursion to very low (−1.5‰) $\delta^{98}Mo_{auth}$ values, associated with relatively high Mo concentrations and a peak in Fe/Al. These $\delta^{98}Mo_{auth}$ values are lower than most published sediment data, but such values have been modeled for deposition in mildly euxinic conditions, with higher scavenging rates for more sulfidized thiomolybdate species (Dahl et al., 2010; Matthews et al., 2017; Sweere et al., 2021). The high Fe and Mo concentrations of these samples suggest that removal as Fe-Mo-S particulates may have been important (Helz and Vorlicek, 2019).

In the late sapropel stages, $\delta^{98}Mo_{auth}$ values rise towards seawater compositions and Mo concentrations are high (>100 ppm). These data reflect deposition in strongly euxinic conditions as found for highly sulfidic (dissolved $[H_2S]_{aq}$ >11 µmol/L; Erickson and Helz, 2000) modern marine basins, where conversion of MoO_4^{2-} to MoS_4^{2-} is nearly complete (e.g. Erickson and Helz, 2000; Neubert et al., 2008; Helz et al., 2011; Nägler et al., 2011). The upper late stage of both S5 and S7 is characterized by falling $[Mo]_{auth}$ and steady $\delta^{98}Mo_{auth}$ of around +2‰ (Fig. 3, 5). Such behavior likely reflects a drawdown of the basinal Mo inventory due to efficient Mo uptake into sediments under strongly euxinic conditions (e.g.

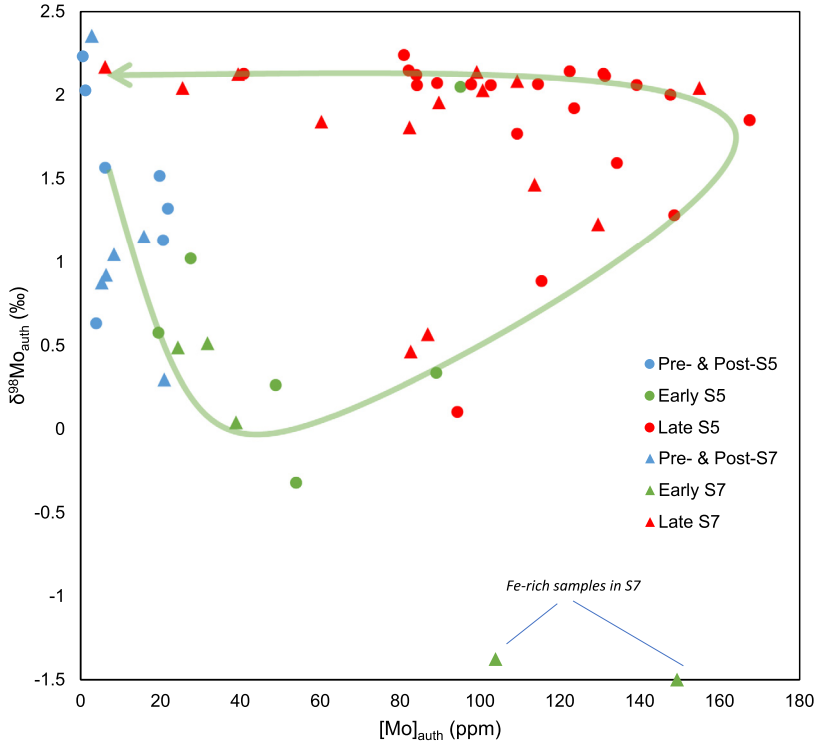

Fig. 5. δ^{98}Mo – $[Mo]_{auth}$ cross plots for sapropels S5 and S7. Green arrow indicates the general temporal evolution through both sapropel events.

Nägler et al., 2011), where particle-reactive MoS_4^{2-} is the dominant dissolved Mo species. Together with more efficient removal, sluggish circulation and the ensuing diminished resupply reduce dissolved [Mo] in the water column, while near-complete conversion to sulfidized phases keeps δ^{98}Mo close to the open-ocean value. Hence, a scatterplot of $\delta^{98}Mo_{auth}$ vs. $[Mo]_{auth}$ shows a flat trend in this late stage (Fig. 5).

In post-sapropel samples, Mo concentrations quickly fall below 25 ppm, (Fig. 3a,e), which suggests non-euxinic conditions (Scott and Lyons, 2012). However, $\delta^{98}Mo_{auth}$ in post-S7 remains close to the seawater value at around +2‰ (Fig. 3g). Such high $\delta^{98}Mo_{auth}$ values together with low $[Mo]_{auth}$ implies Mo conversion to MoS_4^{2-} remains nearly complete, perhaps confined to sulfidic pore waters.

4.3. Behavior of uranium and its isotopes during sapropel events

In contrast to Mo systematics, $[U]_{auth}$ and $\delta^{238}U_{auth}$ show differing trends between S5 and S7 (Fig. 3 b,d,f,h). These differing trends are particularly highlighted by a $[U]_{auth}$ versus δ^{238}U crossplot (Fig. 6). For both events, a $\delta^{238}U_{auth}$ maximum is reached in the lower part of the sapropel, but this occurs for only a minor increase in $[U]_{auth}$, with maximum $[U]_{auth}$ later in the sapropel event. For S5, $\delta^{238}U_{auth}$ increases from an average of −0.25‰ to a first maximum of +0.17‰. A second peak of ∼0‰ is then seen later in the late sapropel. For S7, $\delta^{238}U_{auth}$ starts ∼ −0.24‰ and reaches a higher maximum of ∼ +0.35‰, remaining relatively invariant for the rest of the event.

As discussed in Section 4.1, element concentration data indicate that pre- and early sapropel stages were not strongly reducing. Therefore, $\delta^{238}U_{auth}$ values similar to seawater (−0.39‰) during these stages are unlikely to result from U depletion in the water column, which would only be expected under restricted euxinic settings (e.g. Rolison et al., 2017). Instead, these low $\delta^{238}U_{auth}$ values could be explained by near-quantitative consumption of pore water U during authigenic U sequestration, due to supply-limitation resulting from a "separation zone" between the sediment-water interface and the zone of U reduction (Andersen et al., 2014). Such δ^{238}U values are seen in modern 'hypoxic' margin sediments (Andersen et al., 2016). The smooth $\delta^{238}U_{auth}$ rise in the early stages of the records (Fig. 3) would then reflect a gradual thinning of such a "separation zone". As the chemocline rises through the sediment, the decreased distance between bottom water and the U accumulation zone reduces supply-limitation of U, such that U uptake in pore water becomes less quantitative, and the resulting larger apparent fractionation factor is expressed as higher $\delta^{238}U_{auth}$. Since U reduction is below the Fe(II)–Fe(III) redox boundary and can be mediated by iron- and sulfate-reducing bacteria (Lovley et al., 1991; Zheng et al., 2002), the ascent of the U reduction front towards the sediment-water interface implies that the sulfate-sulfide redoxcline also shoals. In other words, the δ^{238}U data are consistent with redox conditions becoming more reducing during early sapropel development, as also inferred from Mo systematics (Section 4.2).

$\delta^{238}U_{auth}$ values at the end of the early sapropel stage are close to +0.2‰ (+0.17‰ in S5 and +0.26‰ in S7; Fig. 3 d,h). These values are equivalent to an isotopic offset of about +0.6‰ from the open ocean value, and this implies U reduction starting at the sediment-water interface (Andersen et al., 2014), likely coinciding with euxinic bottom water conditions. Indeed, the early stages are interpreted to encompass the transition to euxinia based on enrichments of Fe and Mn (Section 4.1). The water column under such conditions is expected to be free of significant U depletion and thus Eastern Mediterranean bottom waters would have δ^{238}U similar to the open ocean.

During the late sapropel stage in S5, $\delta^{238}U_{auth}$ decreases and then increases slightly until the end of the late stage (Fig. 3d), while $[U]_{auth}$ rises to a plateau above 35 ppm (Fig. 3b). At the same time, elevated $[Mo]_{auth}$ and seawater-like δ^{98}Mo values suggest continued euxinia during this stage of S5 (Section 4.2), indicating that the lower $\delta^{238}U_{auth}$ cannot be ascribed to quantitative drawdown in pore waters associated with a less-reducing "separation zone". Instead, this sedimentary δ^{238}U drop most likely tracks a decrease in the δ^{238}U value of Eastern Mediterranean bottom water, as reduced bottom-water ventilation decreased dissolved U

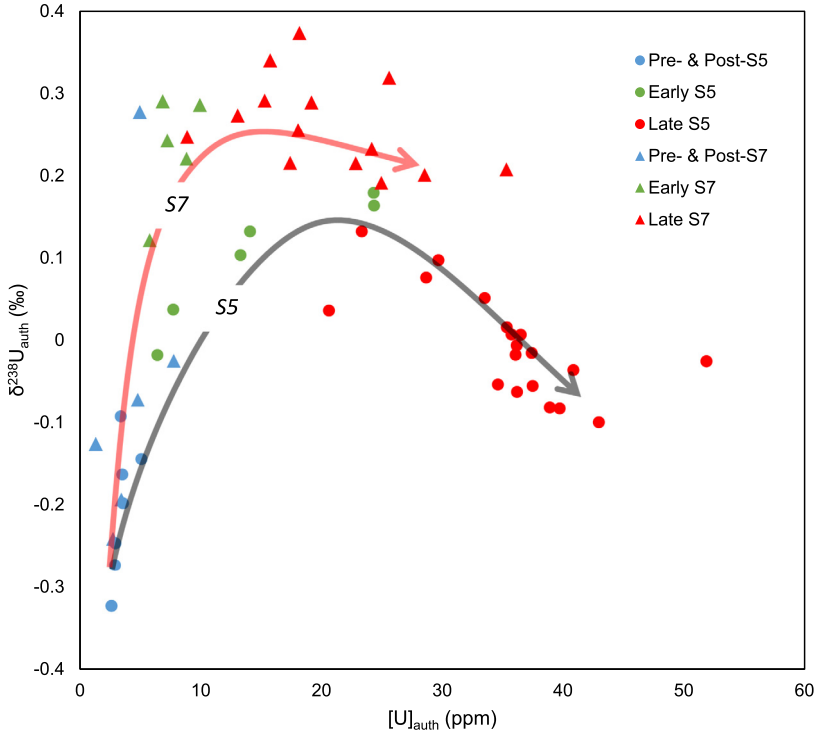

Fig. 6. $\delta^{238}U$ – $[U]_{auth}$ cross plots for sapropels S5 and S7. Gray and red arrows roughly show the temporal evolution through S5 and S7 respectively.

supply and drove U depletion in the water column. In light of the $\delta^{98}Mo$ data, the sedimentary $\delta^{238}U$ trend thus probably indicates diminished Eastern Mediterranean deep-water renewal during late S5, as also suggested by data from the deeper Site 967 (Andersen et al., 2018). The fact that $[U]_{auth}$ increases during this $\delta^{238}U_{auth}$ decrease (Figs. 3b, d; 6) implies stronger U uptake into sediments despite lower concentrations of dissolved U in the bottom water. A similar inverse $\delta^{238}U_{auth}$–$[U]_{auth}$ correlation is also observed in S5 from ODP967 (Andersen et al., 2018), as well as in modern Black Sea euxinic sediments (Rolison et al., 2017; Brüske et al., 2020). The general presence of this characteristic trend could imply that $[U]_{auth}$ is not sensitive to dissolved [U] in this stage, but possibly more influenced by the efficiency of U reduction and accumulation, which are linked to H_2S concentration in the water column via microbial mediation (Lovley et al., 1991).

If the isotopic offset between sedimentary U and dissolved U in bottom water remained constant, the slight $\delta^{238}U$ increase in the upper late S5 implies either: (1) that the bottom water at this locality was replenished with open-ocean U (Andersen et al., 2018; Bura-Nakić et al., 2018), with a $\delta^{238}U$ higher than the modified basin bottom water value; and/or (2) weaker uptake of U into sediments, allowing bottom waters to return to open-ocean values. If $[U]_{auth}$ is not sensitive to dissolved [U], the fact that $[U]_{auth}$ stays close to 40 ppm at this time might suggest fairly stable sedimentary U uptake efficiency. This implies that the slight $\delta^{238}U$ rise in the second half of late S5 is more likely to result from somewhat strengthened bottom-water ventilation at coring site 64PE406-E1. By contrast, the deeper locality of Site 967 on the flank of Hellenic trench (Andersen et al., 2018), where ventilation might be expected to be weaker, does not show the second minor increase in $\delta^{238}U$.

Unlike S5, late S7 has lower $[U]_{auth}$, varying between 20 and 40 ppm, and higher $\delta^{238}U_{auth}$ values. The generally higher $\delta^{238}U$ values for late S7 compared to S5 can be explained by stronger summer insolation during sapropel S5, leading to higher sea surface temperatures and run-off compared to S7 (Emeis et al., 2003; Ziegler et al., 2010), in turn resulting in stronger stratification of the Eastern Mediterranean Sea during S5. However, in the earliest part of this stage, the very high values of $\delta^{238}U_{auth} > +0.3‰$ (Fig. 3h) cannot be explained by changing deep-water renewal rates, but require an isotopic offset larger than the threshold of diffusion-controlled reduction of dissolved U in pore water (+0.6‰; Andersen et al., 2014). Partial U removal in pore water could yield an isotopic offset from seawater over +0.6‰ (Andersen et al., 2014), but the suboxic-anoxic conditions suggested in this scenario would limit authigenic U enrichments, contrary to the observed high enrichments of both Mo and U (Fig. 3e,f) and the evidence of $\delta^{98}Mo$ (Section 4.2). Another mechanism that could produce high $\delta^{238}U$ is U reduction with little or no diffusion limitation, such as U reduction on settling particulate organic matter in the water column, or reduction in highly porous organic flocculent layers at the sediment surface (Andersen et al., 2017, 2020; Cheng et al., 2020). This suggests that a porous benthic organic layer is a more likely potential locus for U reduction in lower late S7, and the build-up of such a layer is at least consistent with elevated productivity during sapropel events (Fig. 2g, h), potentially more similar to the onset of sapropel S1 (Andersen et al., 2020; Clarkson et al., 2021). However, the late S7 interval, with $\delta^{238}U$ values around +0.3‰, is not associated with particularly high TOC contents or Ba/Al values, implying that productivity is not likely to be much higher than the rest of S7. Hence, factors apart from productivity may play a role in determining the deposition of an organic flocculent layer, or the highly elevated $\delta^{238}U$ values may arise from an as-yet unidentified process.

4.4. Interrelationship between Mo and U isotope fractionations

Unlike previous studies in which authigenic $\delta^{238}U$ and $\delta^{98}Mo$ display a simple inverse correlation, shifting towards seawater values under more reducing conditions (Bura-Nakić et al., 2018; Brüske et al., 2020; Kendall et al., 2020), our high-resolution study shows a more complex relationship that holds significant extra information on the development of anoxia into full sapropel conditions. The trajectory of each sapropel in a $\delta^{238}U$–$\delta^{98}Mo$ cross-plot

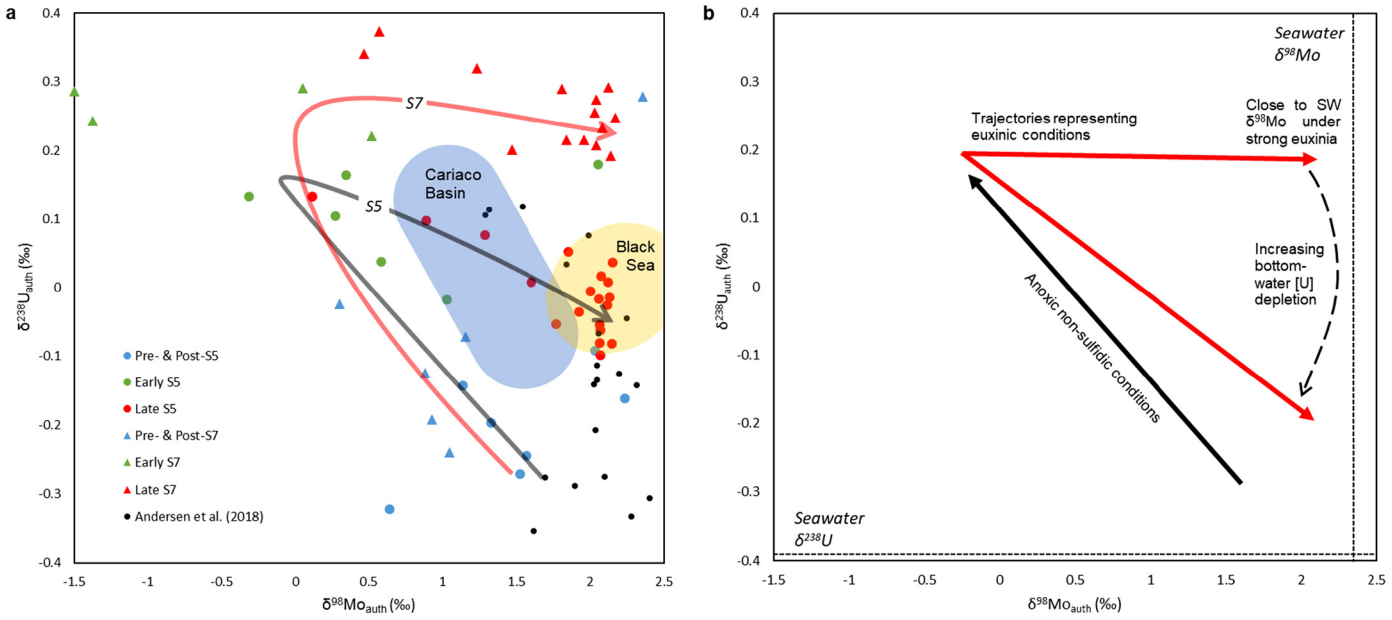

Fig. 7. (a) Isotope compositions of authigenic Mo and U from sapropels S5 (black) and S7 (red) in this study are plotted against each other, with the overall temporal evolution represented by gray and red arrows respectively. S5 data from nearby core ODP967 are indicated by black dots for comparison (retrieved from Andersen et al., 2018). The yellow shaded region denotes the range of δ^{98}Mo and δ^{238}U of most Black Sea samples from at least 3 cm below the tops of cores — 32MUC24, BC21, BC25, BC43, BC55, and 25GC1, while the gray shaded region shows the location of most isotopic data for samples (at least 10 cm below the core top) from the Cariaco Basin (retrieved from Brüske et al., 2020 and references therein). (b) Schematic trajectories show how Mo and U isotope compositions evolve in δ^{98}Mo–δ^{238}U space when the reducing conditions intensify under anoxic non-sulfidic conditions (black arrow) and under euxinic conditions (red arrows). The arrow heads are close to the line of seawater δ^{98}Mo as a result of near-complete sulfidization under strongly euxinic conditions ($[H_2S] > 11$ μM). Their final δ^{238}U-coordinates are lower when the bottom water is more depleted in dissolved U (Andersen et al., 2018) and thus the slope of δ^{98}Mo–δ^{238}U trajectories under euxinic conditions becomes steeper with increasing bottom-water [U] depletion.

(Fig. 7a) can be roughly split into two temporal arrays reflecting early and late sapropel stages. The first, early-stage array is similar for both S5 and S7, with decreasing δ^{98}Mo and increasing δ^{238}U — both away from seawater values — as anoxia intensifies. In the second, late stage array, S5 shows the inverse pattern, with decreasing δ^{238}U for an increase in δ^{98}Mo toward seawater-like values. By contrast, S7 exhibits a trend like S5 for δ^{98}Mo, toward seawater, but δ^{238}U remains invariant around +0.2‰.

The δ^{98}Mo–δ^{238}U relationship observed for early sapropel stages, with isotopic values moving away from seawater values under intensifying reducing conditions, represents a feature that has not previously been captured in lower-resolution records of S5 (e.g. Andersen et al., 2018). A similar δ^{98}Mo–δ^{238}U trend has been observed in sapropel S1 from ODP967 (Andersen et al., 2020), in whose early stages Azrieli-Tal et al. (2014) have used Mo and Fe isotopes and Mo_{EF}-U_{EF} covariation to identify mild euxinia. However, the fact that a similar trend has been interpreted as resulting from (mild) euxinia in S1 does not invalidate our hypothesis regarding anoxic non-sulfidic conditions. The higher δ^{238}U values in S1 (> +0.5‰) were proposed to be the result of an apparent fractionation factor above +0.6‰ due to organic-rich floccule layers, whose occurrence is likely to be controlled by various factors in addition to redox conditions (Andersen et al., 2020).

The second, flatter segments of the δ^{98}Mo-δ^{238}U trends in Fig. 7a represent late sapropels, which are inferred to form under euxinic bottom water conditions (Sections 4.2, 4.3). In both late sapropels, δ^{98}Mo and δ^{238}U gradually become relatively invariant (Fig. 3c,d,g,h), suggesting that the system has likely approached a stable configuration. In δ^{238}U–δ^{98}Mo space, the end of the trajectories (maximum δ^{98}Mo) is at around +2‰ for both sapropels. However, δ^{238}U values at these maximum δ^{98}Mo are different from each other, at around −0.05‰ in S5 and about +0.2‰ in S7 (Fig. 7a). Considering the relationship between bottom-water U depletion and sedimentary $\delta^{238}U_{auth}$ (Bura-Nakić et al., 2018; Andersen et al., 2018), these δ^{238}U values suggest bottom water U depletion of ~40% for S5, and no significant U depletion for S7. Interestingly, the end of the S5 trajectory forms a cluster of data that is within the δ^{238}U–δ^{98}Mo space defined by modern Black Sea sedimentary data (Fig. 7a; Brüske et al., 2020 and references therein). This similarity in isotope ratios, governed ultimately by basinal mass balance for these two elements (Sections 4.2, 4.3), may imply that euxinic conditions associated with slower deep-water renewal during late S5 are comparable to the modern Black Sea. Black Sea-like conditions have also been inferred for S5 based on Fe/Al vs. δ^{56}Fe data from a different core (Benkovitz et al., 2020), supporting the observation that redox conditions and deep-water renewal times of sapropel S5 were likely similar to the modern Black Sea. By contrast, lower $[U]_{auth}$ and a smaller inferred U depletion in S7 suggest reducing conditions that were weaker, or temporally less stable, than both S5 and the modern Black Sea. Fe/Al and δ^{56}Fe data for sapropel S7 support dominantly euxinic conditions for this interval, with some data deviating from trends found for sapropel S5 and the Black Sea also suggesting conditions during S7 were not quite as strongly reducing or stable (Benkovitz et al., 2020).

The late stages of sapropels S5 and S7 are indistinguishable from each other in terms of δ^{98}Mo values, which clearly mark them as bearing significant water-column euxinia. But it is not possible to distinguish between degrees of euxinia or water-mass restriction due to the threshold behavior of Mo sulfidization. Thus, the combination of sedimentary δ^{98}Mo and δ^{238}U data allows a more detailed view of redox and hydrographic changes than can be attained with δ^{98}Mo alone. Such differences in fractionation of Mo and U likely reflect their different behaviors in response to various $[H_2S]$ and degrees of restriction. Mo removal and fractionation are dominantly influenced by dissolved $[H_2S]$, and show step-like behavior, in particular the shift in the dominant dissolved Mo species from molybdate to MoS_4^{2-} at the $[H_2S]_{aq}$ of 11 μM (Helz et al., 1996; Erickson and Helz, 2000). Above this threshold, near-complete sulfidization of Mo results in invariant sedimentary δ^{98}Mo. In other words, δ^{98}Mo can only show significant variation in mildly euxinic conditions ($[H_2S]_{aq} < 11$ μM) or when H_2S is restricted to pore waters.

By contrast, the lack of a direct dependence of U removal rates on degree of euxinia results in a more gradual change of sedimentary δ^{238}U with the extent of basin restriction. If, for simplicity, we only consider sedimentary reduction and fractionation with a constant isotopic offset of +0.6‰ from the bottom-water δ^{238}U, increasing basin restriction and the ensuing water-column U drawdown will lead to a decrease in $\delta^{238}U_{auth}$ values as conditions progress to highly euxinic, and highly restricted. However, it is noteworthy that $\delta^{238}U_{auth}$ near the seawater value of −0.4‰, resulting from near-quantitative U uptake, has only been observed in highly restricted and small-volume euxinic basins, such as Lake Rogoznica and Kyllaren Fjord (Noordmann et al., 2015; Bura-Nakić et al., 2018), and not in the highly euxinic but large Black Sea. This observation implies that there is a wide range of conditions — in both intensity of euxinia and extent of ventilation — before $\delta^{238}U_{auth}$ becomes invariant and stabilizes close to −0.4‰.

In δ^{238}U–δ^{98}Mo space, the combination of the step-like response of Mo and the more gradual response of U results in the different trajectories that we observe for S5 and S7 (Fig. 7a) and that we expect to characterize anoxic events of varying intensity more generally (Fig. 7b). When euxinia is sufficiently strong that water-column Mo is nearly completely sulfidized, sedimentary δ^{98}Mo values will cluster close to that of seawater. However, depending on the degree of restriction and the duration of the event, the steady state δ^{238}U value may be anywhere between +0.2 and −0.4‰ in our simplified scenario. As a consequence of the difference in the timescales of response of the two elemental systems, driven by different reduction and removal mechanisms, the trajectory representing progressive intensification of reducing conditions from mildly euxinic to euxinic steady state will thus be steeper if the bottom-water U depletion is higher (red arrows in Fig. 7b). The co-variation systematics of sedimentary δ^{238}U and δ^{98}Mo can thus constrain the severity and extent of basin restriction events and their consequences for basin redox states.

5. Conclusion and outlook

High-resolution records of Mo-U concentrations and their isotopes from Mediterranean sapropel events S5 and S7 reveal consistent temporal patterns that can be related to the local depositional redox conditions. The large range of δ^{98}Mo values can largely be attributed to the transition from non- to strongly euxinic conditions over the temporal span of these events. Similar stratigraphic δ^{98}Mo patterns are found for both sapropels and between different cores, highlighting the potential of δ^{98}Mo data for reconstructing basin redox and hydrographic conditions. $\delta^{238}U_{auth}$ values also exhibit a wide range, and both stratigraphic δ^{238}U trends start with increasing $\delta^{238}U_{auth}$ values, which likely reveal the control of sedimentary U uptake by separation between bottom water and the U reduction-accumulation front under anoxic non-sulfidic conditions. Shoaling of the sedimentary chemocline can attenuate the reservoir effect of U removal within pore water, resulting in less quantitative drawdown in pore water, and higher authigenic δ^{238}U values. The data presented here raise issues for the reconstruction of global ocean redox conditions using δ^{98}Mo or δ^{238}U in anoxic sediments. Both δ^{98}Mo and δ^{238}U values vary considerably over relatively short timescales, suggesting that the isotope composition of the organic-rich sediment sink in similar environments can only be poorly constrained.

Our high-resolution data also reveal more complex patterns in the δ^{98}Mo–δ^{238}U relationships than previous studies, which suggested increasing δ^{98}Mo and decreasing δ^{238}U values, towards their seawater values, under more reducing conditions (Andersen et al., 2018; Brüske et al., 2020). Our data show that this is preceded by a δ^{98}Mo–δ^{238}U trajectory away from the seawater values during early sapropel development. These lower sapropel sections are inferred to be deposited under increasingly reducing conditions covering transitions from anoxic non-sulfidic to mildly euxinic states, in contrast to the overlying sediments that were likely formed when the water-column was euxinic.

Focusing on the euxinic intervals of the sapropels, during which Mo removal occurs in the water column and U reduction begins at the sediment-water interface, this study shows very different δ^{98}Mo–δ^{238}U trajectory slopes between S5 and S7. δ^{238}U values in the late stage of S7 are elevated relative to S5, despite δ^{98}Mo values close to the seawater value in both cases. This difference in δ^{238}U can be attributed to the different degrees of bottom-water depletion in dissolved U, which are influenced by the deep-water renewal timescale and the U uptake rate. Hence, if the bottom water is euxinic enough to attain near-quantitative Mo drawdown, the bottom-water [U] depletion could determine the slope of δ^{98}Mo–δ^{238}U trajectory (Fig. 7b), thus allowing use of the combined δ^{98}Mo–δ^{238}U systematics to distinguish between different stages of restriction among highly euxinic settings. Our findings thus reveal the added value of combining δ^{98}Mo and δ^{238}U, at high resolution, for paleoredox reconstruction.

CRediT authorship contribution statement

Chun Fung Chiu: Conceptualization, Data curation, Investigation, Methodology, Visualization, Writing – original draft. **Tim C. Sweere:** Conceptualization, Data curation, Investigation, Methodology, Resources, Supervision, Validation, Writing – review & editing. **Matthew O. Clarkson:** Investigation, Methodology, Resources, Supervision, Validation, Writing – review & editing. **Gregory F. de Souza:** Conceptualization, Methodology, Supervision, Writing – review & editing. **Rick Hennekam:** Resources, Writing – review & editing. **Derek Vance:** Conceptualization, Funding acquisition, Project administration, Writing – review & editing.

Declaration of competing interest

The authors declare that they have no known competing financial interests or personal relationships that could have appeared to influence the work reported in this paper.

Acknowledgements

We thank chief-scientist Marcel van der Meer and the crew of the R/V Pelagia for obtaining the 64PE406-E1 core material during the NESSC cruise. We would also like to thank Corey Archer and Madalina Jaggi for laboratory assistance at ETHZ. The Netherlands Earth System Science Centre (NESSC) program is carried out under financial support by the Ministry of Education, Culture and Science (OCW; Grant 024.002.001). TCS has received funding from the European Union's Horizon 2020 research and innovation programme under the Marie Skłodowska-Curie grant agreement No. 834236. Further ETH involvement in this research was supported by the Swiss National Science Foundation (SNF) through grant 200021_184873/1 (to DV). We thank two anonymous reviewers and editor Frederic Moynier for their helpful and constructive comments and handling of the manuscript.

Appendix A. Supplementary material

Supplementary material related to this article can be found online at https://doi.org/10.1016/j.epsl.2022.117527.

References

Algeo, T.J., Tribovillard, N., 2009. Environmental analysis of paleoceanographic systems based on molybdenum-uranium covariation. Chem. Geol. 268, 211–225.

Andersen, M.B., Romaniello, S., Vance, D., Little, S.H., Herdman, R., Lyons, T.W., 2014. A modern framework for the interpretation of $^{238}U/^{235}U$ in studies of ancient ocean redox. Earth Planet. Sci. Lett. 400, 184–194.

Andersen, M.B., Vance, D., Morford, J.L., Bura-Nakić, E., Breitenbach, S.F.M., Och, L., 2016. Closing in on the marine $^{238}U/^{235}U$ budget. Chem. Geol. 420, 11–22.

Andersen, M.B., Stirling, C.H., Weyer, S., 2017. Uranium isotope fractionation. Rev. Mineral. Geochem. 82, 799–850.

Andersen, M.B., Matthews, A., Vance, D., Bar-Matthews, M., Archer, C., de Souza, G.F., 2018. A 10-fold decline in the deep Eastern Mediterranean thermohaline overturning circulation during the last interglacial period. Earth Planet. Sci. Lett. 503, 58–67.

Andersen, M.B., Matthews, A., Bar-Matthews, M., Vance, D., 2020. Rapid onset of ocean anoxia shown by high U and low Mo isotope compositions of sapropel S1. Geochem. Perspect. Lett. 15, 10–14.

Anderson, R.F., Fleisher, M.Q., LeHuray, A.P., 1989. Concentration, oxidation state, and particulate flux of uranium in the Black Sea. Geochim. Cosmochim. Acta 53, 2215–2224.

Archer, C., Vance, D., 2008. The isotopic signature of the global riverine molybdenum flux and anoxia in the ancient oceans. Nat. Geosci. 1, 597–600.

Azrieli-Tal, I., Matthews, A., Bar-Matthews, M., Almogi-Labin, A., Vance, D., Archer, C., Teutsch, N., 2014. Evidence from molybdenum and iron isotopes and molybdenum-uranium covariation for sulphidic bottom waters during Eastern Mediterranean sapropel S1 formation. Earth Planet. Sci. Lett. 393, 231–242.

Barling, J., Anbar, A.D., 2004. Molybdenum isotope fractionation during adsorption by manganese oxides. Earth Planet. Sci. Lett. 217, 235.

Benkovitz, A., Matthews, A., Teutsch, N., Poulton, S.W., Bar-Matthews, M., Almogi-Labin, A., 2020. Tracing water column euxinia in Eastern Mediterranean sapropels S5 and S7. Chem. Geol. 545, 119627. https://doi.org/10.1016/j.chemgeo.2020.119627.

Brüske, A., Weyer, S., Zhao, M.-Y., Planavksy, N.J., Wegwerth, A., Neubert, N., Dellwig, O., Lau, K.V., Lyons, T.W., 2020. Correlated molybdenum and uranium isotope signatures in modern anoxic sediments: implications for their use as paleoredox proxy. Geochim. Cosmochim. Acta 270, 449–474.

Bura-Nakić, E., Andersen, M.B., Archer, C., de Souza, G.F., Margus, M., Vance, D., 2018. Coupled Mo-U abundances and isotopes in a small marine euxinic basin: constraints on processes in euxinic basins. Geochim. Cosmochim. Acta 222, 212–229.

Chappaz, A., Lyons, T.W., Gregory, D.D., Reinhard, C.T., Gill, B.C., Li, C., Large, R.R., 2014. Does pyrite act as an important host for molybdenum in modern and ancient euxinic sediments? Geochim. Cosmochim. Acta 126, 112–122.

Cheng, M., Li, C., Jin, C., Wang, H., Algeo, T.J., Lyons, T.W., Zhang, F., Anbar, A., 2020. Evidence for high organic carbon export to the early Cambrian seafloor. Geochim. Cosmochim. Acta 287, 125–140. https://doi.org/10.1016/j.gca.2020.01.050.

Clarkson, M.O., Hennekam, R., Sweere, T.C., Andersen, M.B., Reichart, G.-J., Vance, D., 2021. Carbonate associated uranium isotopes as a novel local redox indicator in oxidatively disturbed reducing sediments. Geochim. Cosmochim. Acta 311, 12–28.

Dahl, T.W., Anbar, A.D., Gordon, G.W., Rosing, M.T., Frei, R., Canfield, D.E., 2010. The behavior of molybdenum and its isotopes across the chemocline and in the sediments of sulfidic Lake Cadagno, Switzerland. Geochim. Cosmochim. Acta 74, 144–163.

de Lange, G.J., Thomson, J., Reitz, A., Slomp, C.P., Speranza Principato, M., Erba, E., Corselli, C., 2008. Synchronous basin-wide formation and redox-controlled preservation of a Mediterranean sapropel. Nat. Geosci. 1 (9), 606–610.

Dunk, R.M., Mills, R.A., Jenkins, W.J., 2002. A reevaluation of the oceanic uranium budget for the Holocene. Chem. Geol. 190, 45–67.

Emeis, K.-C., Schulz, H., Struck, U., Rossignol-Strick, M., Erlenkeuser, H., Howell, M.W., Kroon, D., Mackensen, A., Ishizuka, S., Oba, T., Sakamoto, T., Koizumi, I., 2003. Eastern Mediterranean surface water temperatures and $\delta^{18}O$ composition during deposition of sapropels in the late Quaternary. Paleoceanography 18 (1).

Emerson, S.R., Huested, S.S., 1991. Ocean anoxic and the concentration of molybdenum and vanadium in seawater. Mar. Chem. 34, 177–196.

Erickson, B.E., Helz, G.R., 2000. Molybdenum(VI) speciation in sulfidic waters: stability and lability of thiomolybdates. Geochim. Cosmochim. Acta 64, 1149–1158.

Goldberg, T., Archer, C., Vance, D., Poulton, S.W., 2009. Mo isotope fractionation during adsorption to Fe (oxyhydr)oxides. Geochim. Cosmochim. Acta 73, 6502–6516.

Grant, K.M., Grimm, R., Mikolajewicz, U., Marion, G., Ziegler, M., Rohling, E.J., 2016. The timing of Mediterranean sapropel deposition relative to insolation, sea-level and African monsoon changes. Quat. Sci. Rev. 140, 125–141.

Helz, G.R., Miller, C.V., Charnock, J.M., Mosselmans, J.F.W., Pattrick, R.A.D., Garner, C.D., Vaughan, D.J., 1996. Mechanism of molybdenum removal from the sea and its concentration in black shales. Geochim. Cosmochim. Acta 60, 3631–3642.

Helz, G.R., Bura-Nakić, E., Mikac, N., Ciglenecki, I., 2011. New model for molybdenum behavior in euxinic waters. Chem. Geol. 284, 323–332.

Helz, G.R., Vorlicek, T.P., 2019. Precipitation of molybdenum from euxinic waters and the role of organic matter. Chem. Geol. 509, 178–193.

Hennekam, R., van der Bolt, B., van Nes, E.H., de Lange, G.J., Scheffer, M., Reichart, G.-J., 2020. Early-warning signals for marine anoxic events. Geophys. Res. Lett. 47, e2020GL089183. https://doi.org/10.1029/2020GL089183.

Huckriede, H., Meischner, D., 1996. Origin and environment of manganese-rich sediments within black-shale basins. Geochim. Cosmochim. Acta 60, 1399–1413.

Kendall, B., Komiya, T., Lyons, T.W., Bates, S.M., Gordon, G.W., Romaniello, S.J., Jiang, G., Creaser, R.A., Xiao, S., McFadden, K., Sawaki, Y., Tahata, M., Shu, D., Han, J., Li, Y., Chu, X., Anbar, A.D., 2015. Uranium and molybdenum isotope evidence for an episode of widespread ocean oxygenation during the late Ediacaran Period. Geochim. Cosmochim. Acta 156, 173–193.

Kendall, B., Dahl, T.W., Anbar, A.D., 2017. The stable isotope geochemistry of molybdenum. Rev. Mineral. Geochem. 82 (1), 683–732.

Kendall, B., Wang, J., Zheng, W., Romaniello, S., Over, J., Bennett, Y., Xing, L., Kunert, A., Boyes, C., Liu, J., 2020. Inverse correlation between the molybdenum and uranium isotope compositions of Upper Devonian black shales caused by changes in local depositional conditions rather than global ocean redox variations. Geochim. Cosmochim. Acta 287, 141–164.

Kerl, C.F., Lohmayer, R., Bura-Nakić, E., Vance, D., Planer-Friedrich, B., 2017. Experimental confirmation of isotope fractionation in thiomolybdates using ion chromatographic separation and detection by multicollector ICPMS. Anal. Chem. 89, 3123–3129.

Lovley, D.R., Phillips, E.J., Gorby, Y.A., Landa, E.R., 1991. Microbial reduction of uranium. Nature 350 (6317), 413–416.

Lyons, T.W., Severmann, S., 2006. A critical look at paleoredox proxies: new insights from modern euxinic marine basins. Geochim. Cosmochim. Acta 70, 5698–5722.

Matthews, A., Azrieli-Tal, I., Benkovitz, A., Bar-Matthews, M., Vance, D., Poulton, S.W., Teutsch, N., Almogi-Labin, A., Archer, C., 2017. Anoxic development of sapropel S1 in the Nile Fan inferred from redox sensitive proxies, Fe speciation, Fe and Mo isotopes. Chem. Geol. 475, 24–39.

Melki, T., Kallel, N., Fontugne, M., 2010. The nature of transitions from dry to wet condition during sapropel events in the Eastern Mediterranean Sea. Palaeogeogr. Palaeoclimatol. Palaeoecol. 291, 267–285.

Miller, C.A., Peucker-Ehrenbrink, B., Walker, B.D., Marcantonio, F., 2011. Re-assessing the surface cycling of molybdenum and rhenium. Geochim. Cosmochim. Acta 75, 7146–7179.

Nägler, T.F., Neubert, N., Böttcher, M.E., Dellwig, O., Schnetger, B., 2011. Mo isotope fractionation in pelagic euxinia: results from the modern Black and Baltic Seas. Chem. Geol. 289, 1–11.

Neubert, N., Nägler, T.F., Böttcher, M.E., 2008. Sulfidity controls molybdenum isotope fractionation into euxinic sediments: evidence from the modern Black Sea. Geology 36, 775–778.

Noordmann, J., Weyer, S., Montoya-Pino, C., Dellwig, O., Neubert, N., Eckert, S., 2015. Uranium and molybdenum isotope systematics in modern euxinic basins: case studies from the central Baltic Sea and the Kyllaren fjord (Norway). Chem. Geol. 396, 182–195.

Poulson-Brucker, R.L., McManus, J., Severmann, S., Berelson, W.M., 2009. Molybdenum behavior during early diagenesis: insights from Mo isotopes. Geochem. Geophys. Geosyst. 10, Q06010. https://doi.org/10.1029/2008GC002180.

Reitz, A., Wille, M., Nägler, T.F., de Lange, G.J., 2007. Atypical Mo isotope signatures in eastern Mediterranean sediments. Chem. Geol. 245, 1–8.

Richter, S., Alonso-Munoz, A., Eykens, R., Jacobsson, U., Kuehn, H., Verbruggen, A., Aregbe, Y., Wellum, R., Keegan, E., 2008. The isotopic composition of natural uranium samples—measurements using the new $n(^{233}U)/n(^{236}U)$ double spike IRMM-3636. Int. J. Mass Spectrom. 269, 145–148.

Rohling, E.J., Marino, G., Grant, K.M., 2015. Mediterranean climate and oceanography, and the periodic development of anoxic events (sapropels). Earth-Sci. Rev. 143, 62–97.

Rolison, J.M., Stirling, C.H., Middag, R., Rijkenberg, M.J.A., 2017. Uranium stable isotope fractionation in the Black Sea: modern calibration of the $^{238}U/^{235}U$ paleoredox proxy. Geochim. Cosmochim. Acta 203, 69–88.

Scott, C., Lyons, T.W., 2012. Contrasting molybdenum cycling and isotopic properties in euxinic versus non-euxinic sediments and sedimentary rocks: refining the paleoproxies. Chem. Geol. 324–325, 19–27.

Stylo, M., Neubert, N., Wang, Y., Monga, N., Romaniello, S.J., Weyer, S., Bernier-Latmani, R., 2015. Uranium isotopes fingerprint biotic reduction. Proc. Natl. Acad. Sci. 112, 5619–5624.

Sweere, T.C., Hennekam, R., Vance, D., Reichart, G.J., 2021. Molybdenum isotope constraints on H2S build-up during Mediterranean sapropel intervals. Geochem. Perspect. Lett. 17, 16–20.

Tossel, J.A., 2005. Calculating the partitioning of the isotopes of Mo between oxic and sulfidic species in aqueous solutions. Geochim. Cosmochim. Acta 69, 2981–2993.

Tribovillard, N., Algeo, T.J., Lyons, T., Riboulleous, T., 2006. Trace elements as paleoredox and paleoproductivity proxies: an update. Chem. Geol. 232, 12–32.

van Santvoort, P.J.M., De Lange, G.J., Thomson, J., Cussen, H., Wilson, T.R.S., Krom, M.D., Ströhle, K., 1996. Active post-depositional oxidation of the most recent sapropel (S1) in sediments of the eastern Mediterranean Sea. Geochim. Cosmochim. Acta 60 (21), 4007–4024.

Wasylenki, L.E., Rolfe, B.A., Weeks, C.L., Spiro, T.G., Anbar, A.D., 2008. Experimental investigation of the effects of temperature and ionic strength on Mo isotope fractionation during adsorption to manganese oxides. Geochim. Cosmochim. Acta 72, 5997–6005.

Wehausen, R., Brumsack, H.-J., 1999. Cyclic variations in the chemical composition of eastern Mediterranean Pliocene sediments: a key for understanding sapropel formation. Mar. Geol. 153, 161–176.

Zheng, Y., Anderson, R.F., van Geen, A., Fleischer, M.Q., 2002. Remobilization of authigenic uranium in marine sediments by bioturbation. Geochim. Cosmochim. Acta 66, 1759–1772.

Ziegler, M., Tuenter, E., Lourens, L.J., 2010. The precession phase of the boreal summer monsoon as viewed from the eastern Mediterranean (ODP site 968). Quat. Sci. Rev. 29, 1481–1490.